

2

MOLECULAR MODELING OF BIOMEMBRANES: A HOW-TO APPROACH

Allison N. Dickey* and Roland Faller
*Department of Chemical Engineering and Materials Science,
University of California Davis*

2.1. INTRODUCTION TO MOLECULAR DYNAMICS

Computer Simulations have become an important complementary technique to experiment and analytical theory for scientific discoveries. Molecular Dynamics (MD) is one of the most abundant techniques of computer modeling, and is frequently used simulation methods in biomolecular applications. Its popularity may stem from its simplicity and versatile applicability. The fundamental underlying assumption of MD is that the system consists of particles that interact via the classical equations of motion, i.e., both quantum mechanical and relativistic effects are neglected. The exclusion of these effects, however, does not generally have a significant impact on the biomolecular questions being studied.

The simplest equation of motion is Newton's equation, which states that the force acting on a particle is the product of its mass and its acceleration:

$$\vec{F} = m\vec{a}. \quad (2.1)$$

Assuming furthermore that we have only conservative forces in our system, i.e., we neglect friction and any velocity dependent forces, we can write the force as the negative gradient of a potential function that now depends only on the particle positions

$$\vec{F}_i = -\nabla_i V(\{\vec{r}_j\}). \quad (2.2)$$

Address correspondence to Roland Faller, Department of Chemical Engineering and Materials Science, University of California Davis, Bainer Hall, One Shields Avenue, Davis, CA 95616, USA, 530 752-5839, 530 752-1031 (fax), <rfaller@ucdavis.edu>. *Current address: Chemical and Biological Engineering Department, Northwestern University, Evanston, IL 60208, USA.

The gradient here is taken with respect to the position of particle i . Since the acceleration is the second time derivative of particle position, a combination of Eqs. (2.1) and (2.2) leads to a second-order partial differential equation:

$$m\partial_{r_i}^2\vec{r}_i = -\partial_{r_i}V(\{\vec{r}_j\}). \quad (2.3)$$

Even though Newton's equations are not linked to statistical or thermodynamical properties and cannot be extended to include quantum mechanical variables like Hamilton's equations, for the systems that we will discuss here Hamilton's equations reduce to the same Eq. (2.3), and so we will not go through the more complex derivation. Through the use of an integrator, MD solves the second-order PDE in Eq. (2.3) iteratively, where the positions and velocities (or momenta) of all the particles at one time point are used as the initial conditions.

An integrator is an algorithm that solves the PDE by iterative integration, and there are several varieties commonly used in MD. Here we will discuss the Verlet integrator [1] as a prototypical example. The Verlet algorithm has several advantages: it is time inversion symmetric as well as symplectic. These characteristics are required for the correct statistical mechanical behavior of the ensuing ensemble, and the interested reader is referred to several excellent books for a more detailed discussion of MD [2–4].

Most integrators are based on a Taylor expansion of the positions in time:

$$\vec{r}(t) = \sum_{i=0}^{\infty} \partial_{t_i}^i \vec{r}_{t=t_0} \frac{(t-t_0)^i}{i!}. \quad (2.4)$$

For the Verlet integrator, this expansion is performed to the third order, and the first derivative of position is velocity and the second derivative of position is acceleration. For symmetry reasons, the expansion is performed in positive and negative time. If $\Delta t = t - t_0$, the forward and backward expansions are

$$\vec{r}(t = t_0 + \Delta t) = \vec{r}(t_0) + \vec{v}(t_0)\Delta t + \frac{1}{2}\vec{a}(t_0)\Delta t^2 + \frac{1}{6}\partial_t^3\vec{r}(t_0)\Delta t^3 + O(\Delta t^4), \quad (2.5a)$$

$$\vec{r}(t = t_0 - \Delta t) = \vec{r}(t_0) - \vec{v}(t_0)\Delta t + \frac{1}{2}\vec{a}(t_0)\Delta t^2 - \frac{1}{6}\partial_t^3\vec{r}(t_0)\Delta t^3 + O(\Delta t^4). \quad (2.5b)$$

If the forward and the backward expansions are combined, the position Verlet algorithm (Eq. (2.6)) is obtained, and it is exact to the 4th order in the timestep Δt . The position Verlet algorithm predicts the atomic positions at the next timestep given that the atomic positions at the current and previous timesteps are known:

$$\vec{r}(t_0 + \Delta t) = 2\vec{r}(t_0) - \vec{r}(t_0 - \Delta t) + \vec{a}(t_0)\Delta t^2 + O(\Delta t^4). \quad (2.6)$$

Here the velocity is not explicitly represented but rather computed as a difference between positions.

2.2. SPECIFICS OF THE MOLECULAR MODELING OF BIOMEMBRANES

We now focus on biomembrane simulation specifics, where biological systems that span a variety of length scales have been commonly studied using MD over the last two decades [5–13]. Even so, simulation details must still be carefully selected, as it has been found that unfortunate choices in conditions or parameters can lead to unsuccessful simulations [14–16].

In an all-atom simulation, every atom is represented in the model by one interaction center. All atom simulations are very abundant and give the highest possible degree of detail (except for quantum chemical calculations). However, one downfall to a simulation having this degree of accuracy is that they are limited in both the length of simulation time as well as the system size. In biomembrane simulations, this is especially apparent for fully hydrated phospholipid bilayers. Even though the system of interest is the lipid bilayer, a considerable amount of computational effort is spent on simulating the water molecules, which are needed to accurately represent a cellular bilayer. In order to minimize the computational resources that are spent on water molecules, several approaches, such as solvent free bilayer models that use special interactions to mimic water [11,17] and coarse-grained models [18–20], have been devised that allow for the use of larger timescales. Most biomembrane simulations have been performed on free-standing bilayers in water, although a few freestanding monolayers [21–23] and supported bilayers [24,25] have been examined as well.

Biomembranes are inherently anisotropic, and this property needs to be reproduced in the model. Most simulations are performed with periodic boundary conditions, i.e., the simulation box is surrounded by replicas of itself in all directions, which leads to an infinitely extended periodic system. In order to maintain a constant pressure, the simulation volume size needs to fluctuate since pressure and volume are conjugate thermodynamic variables. However, because Newton's equations of motion conserve volume, the pressure has to be controlled via a barostat. Similar in spirit to barostats are thermostats, which modify the system temperature, and further discussion of temperature-controlling techniques can be found elsewhere. A commonly used barostat is the Berendsen, or weak-coupling, barostat [26]. This technique compares an instantaneous pressure with a predefined target pressure, and if the values differ (and they generally do), the box volume and all particle positions are rescaled according to

$$\frac{V_{\text{new}}}{V_{\text{old}}} = \frac{\Delta t}{\tau} \left(1 + \frac{p}{p_{\text{target}}} \right). \quad (2.7)$$

The parameter τ represents the correlation time and should be chosen judiciously. A large correlation time will lead to weaker coupling than a short correlation time. Typical values are on the order of a few ps, with 1 fs being a common choice of timestep for atomistic simulations. The timestep has to be an order of magnitude shorter than the smallest characteristic time found in the system, which typically corresponds to bond or angle vibrations (on the order of 10 fs). If both a thermostat and a barostat are used, their respective correlation times should differ by an order of magnitude as well, with the pressure correlation time having a larger value. If the barostat results in box volume fluctuations, the thickness and area of a membrane become coupled. To avoid this, we independently couple the three axes to the external pressure to reproduce a tension-free bilayer. Of course, the axes (normal and lateral to the membrane) can be coupled

separately to different values, which would produce an overall surface tension. For this situation we have to measure the instantaneous pressure tensor rather than the isotropic pressure.

The overall charge of a simulated system has to be zero. However, biomembrane simulations usually contain charged atoms, and electrostatic interactions differ from most other modeled interactions in that they are long ranged. A long-ranged interaction means that the integral of the potential (which we for simplicity assume to be spherically symmetric) over all space diverges:

$$\int_0^{\infty} V(r)r^2 dr = \infty. \quad (2.8)$$

In contrast to this, the integral for the Lennard-Jones and other short-range interactions converges. A problem with long-ranged interactions stems now from periodic boundary conditions. We cannot neglect charges outside the box. A number of ways to address this have been developed. One of the most successful is the Particle Mesh Ewald [27] technique. The main idea behind this method is that every charged interaction below a certain cutoff is calculated directly. For interactions that do not fall within this cutoff, the interactions are calculated in Fourier space. For the exact implementation we again refer to specialized literature. A second method is the reaction field technique. In this case, a charge interacts with all neighboring charges that fall within a cutoff radius at full strength. However, the charge will only feel an effective dielectric medium for electrostatic interactions whose distance separations exceed the cutoff radius. This may not be the most accurate method, however, since the variety of atom types present in biomembrane simulations leads to a wide range of dielectric values. For example, water has a dielectric constant of ~ 80 and the inner part of a membrane around 2-4. Hence, it is generally advisable for atomistic simulations to use PME for electrostatic calculations.

2.3. FORCE FIELDS: SIMULATION MODELS

Here we discuss some frequently used lipid bilayer models. Many simulations that retain atomistic level detail consist of 128 fully hydrated lipids, with 64 lipids per leaflet. A few studies also examine lipid bilayer structural changes that accompany a reduced level of hydration [28,29]. DPPC (dipalmitoylphosphatidylcholine) is the most abundantly studied lipid [30], and lipids that differ in the saturation or number of carbons in the acyl chains have also been well studied [30–32]. One of the most commonly used phosphatidylcholine (PC) force fields was developed by Berger et al. [33]. Force fields for non-PC lipids, such as phosphatidylserine [34], sphingomyelin [35,36], phosphatidylglycerol [31,32,37], phosphatidylethanolamine [37,38], dimyristoyltrimethylammonium propane [39], and phosphatidic acid [32], have also been published. Sterols, mainly cholesterol [36,40–42] and ergosterol [42,43] but also lanosterol [42], have been modeled. Several websites offer downloadable lipid configurations and topologies to users, and these models contain intra- and intermolecular interactions. The intramolecular bond and angle terms are typically modeled via a harmonic potential. Bonds may also be constrained using algorithms such as LINCS [44] and SHAKE [45]. The torsional degrees of freedom are most often represented by a Fourier series in order to satisfy the required 360° symmetry. Torsions are the most important part of the intramolecular potential, and they are often based on quantum chemical calculations. In some cases, such as for double bonds, special potentials,

such as harmonic dihedrals, are used to help avoid unphysical local conformers. The intramolecular interactions serve a twofold purpose, where they define both the molecule geometry as well as energy differences between different local conformations.

The non-bonded Lennard-Jones interactions are modeled for atom pairs that belong to different molecules as well as for atom pairs that belong to the same molecule but are located a few bonds apart (e.g., at least 3). The Lennard-Jones potential contains two parts. A long-range attractive r^{-6} term comes from the fluctuating dipole London interactions and a short-range repulsive r^{-12} term models the Pauli repulsion. As there is no analytical form for the repulsive segment, the potential is chosen for computational convenience as r^{-12} is just the square of r^{-6} and computing the square is computationally cheap.

We would like to include here a brief discussion on the use of water models. Water is not only important in biomembrane simulations because it is an important constituent of cellular environments, but it is also a unique and interesting compound that has chemical and physical characteristics that lead to complex phase behavior. Most models are adjusted to represent liquid water at ambient conditions and do not necessarily reproduce accurate descriptions of the solid phases. This can be problematic in studies involving low temperatures where freezing becomes important. There is therefore no single “best” water model. The most commonly used water model that is employed in conjunction with standard lipid force fields is the SPC model [46,47]. In this model only the oxygen has a Lennard-Jones interaction site and the two hydrogen atoms only serve as charge sites. In general, one has to be careful to choose a water model that “matches” the chosen lipid model.

2.4. DEGREE OF DETAIL: ATOMISTIC VERSUS COARSE-GRAINED

A number of computational techniques and models have been developed to study a variety of systems of interest. Atomistic models accurately describe not only the molecular structure but also the chemical bonding, electrostatic, and van der Waals interactions. Because of the interaction scale, atomistic models employ a time step that can be as short as a tenth of the period of the fastest mode in the system [48], which often corresponds to a covalent bond or angle stretch. Atomistic models include at least every non-hydrogen atom into the system, and with the short time step atomistic simulations can model membranes that are a few tens of nanometers in size. These simulations often consist of tens of nanoseconds of data and the simulation jobs can be submitted to large-scale computing facilities. Atomistic simulations are widely used in the study of the local structure and dynamics of membranes [49–51]. They can also be used to determine how a particular component, such as sterols, affects membrane structure [52,53]. In most atomistic simulations, nonpolar hydrogens are neglected, i.e., they are subsumed into neighboring heavy atoms, which leads to a united atom description.

Since events such as self-assembly, phase transitions and phase separations occur on length and timescales beyond atomistic capabilities, coarse-grained (CG) or mesoscale models have to be applied to reach the relevant size and time periods. Reducing the degrees of freedom by combining several atoms into one effective particle and eliminating short-range dynamics are two techniques included in CG models that speed up simulations and allow access to collective phenomena [54–60]. One widely used coarse-grained model for lipids is the MARTINI model [18,61], and we refer the reader to the original literature for the exact interaction parameters

between the lipids and the water molecules. We mention here only that 4–6 heavy atoms are represented by one interaction sites and that the coarse-grained parameters are chosen to reproduce important properties of lipid membranes. This model has been effectively used in the study of phase behavior [8,62] and supported membranes [25]. Vesicle fusion and formation [63], as well as hexagonal phase formation [59], have been captured at the molecular level and the phase behavior of several lipid mixtures has been semiquantitatively reproduced [58,64,65]. It has been noted that the increase in dynamics in the CG models is due to the CG molecules being “smoother” than the atomistic molecules, i.e., they exhibit less friction. In the Martini model, the dynamics are a factor of 4 faster than those of atomistic simulations and experiments, where the speed-up was determined through diffusion coefficient comparisons [18]. The phase behavior and pressure–area isotherms are reproduced semiquantitatively, i.e., within 20–30 K [66], and the model uses a reaction field for electrostatics with a dielectric constant of 20. The CG model allows the use of a time step of 40 fs and one CG-water represents 4 real waters.

Less detailed models than the Martini model exist, where water is not explicitly taken into account [11,17,67,68]. The motivation for using such models is to avoid the use of significant amounts of computational time on simulating water molecules. When examining phenomena that occur on large time and length scales, the behavior of the water molecules is usually not a primary interest of the study. To obtain the self-assembly of lipids into a fluid bilayer, the normal Lennard-Jones interaction model needs to be modified, and as an example we briefly discuss a model proposed by Cooke et. al. [11,69,70], where interactions between tail beads are represented as

$$V_{\text{att}}(r) = -\varepsilon, \quad r < r_c, \quad (2.9a)$$

$$V_{\text{att}}(r) = -\varepsilon \cos^2 \frac{\pi(r - r_c)}{2w_c}, \quad r_c < r < r_c + w_c, \quad (2.9b)$$

$$V_{\text{att}}(r) = 0, \quad r > r_c + w_c. \quad (2.9c)$$

The interactions between the head beads as well as between the head and tail beads follows a purely repulsive version of Lennard-Jones that we obtain by cutting off the potential in its minimum and shifting it to zero at that point (WCA potential) [71].

The model uses a tunable long-range weakly varying attractive potential that reproduces a fluid bilayer with properties that are commensurate with experimentally measured values [11].

Further coarse-graining leads to the realm of two-dimensional models, where, for example, one leaflet of a membrane is modeled using hard disks with the sole parameter being the excluded volume (or, more precisely, area). This type of model has been used to study a dipalmitoyl phosphatidylethanolamine (DPPE) and ganglioside GM₁ mixture [72]. A circular excluded area of 45 Å² was used for DPPE and an area of 65 Å² was used for GM₁ and these values were based on experimental pressure–area isotherms for each lipid [73]. GM₁ however, in low to intermediate density mixtures with DPPE does not strongly change the overall area per molecule. Hence, a minimum packing area of 40 Å² per molecule was used for GM₁ in conjunction with DPPE molecules, which leads to the peculiar situation of a binary hard-disk fluid having a cross-interaction radius that is not the average of the self-interaction radii.

2.5. VISUALIZATIONS

It is always a good idea to visualize a simulation system, from either output that is generated during a run or once the simulation has completed. Most simulation packages can write atom coordinates into a protein databank file that can be easily visualized with a number of software packages [74,75]. Visualizing a simulation system, especially in the initial equilibration phase, can serve as a check that the membrane configuration remains intact. The images also provide a convenient method for closely examining the interactions between molecules in a particular region of the system. [Figure 2.1](#) shows images from different regions of a POPA (palmitoyl oleyl phosphatidic acid) lipid bilayer [32].

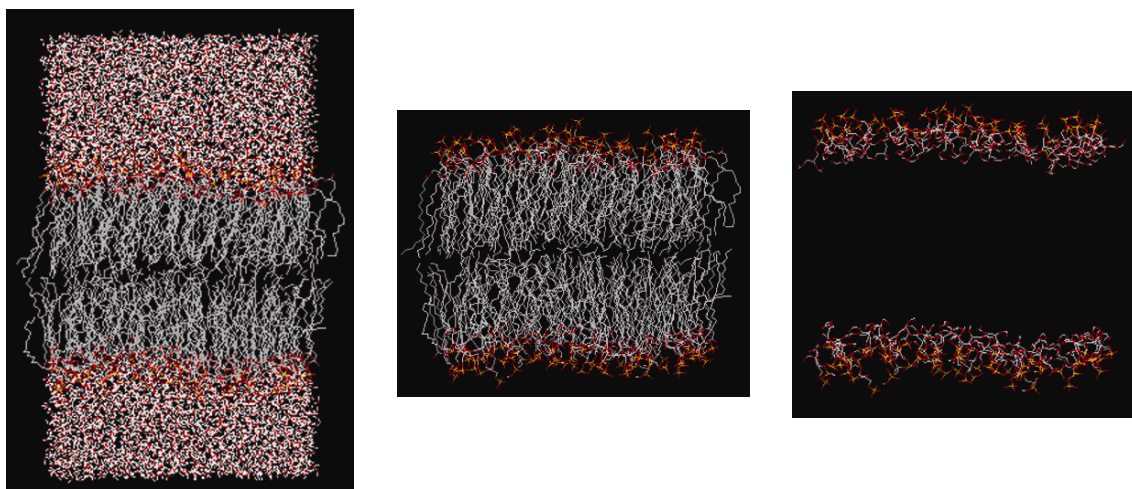


Figure 2.1. Visualization of a POPA lipid bilayer [32]. Left: The system contains 128 lipids with 5443 water molecules. Middle: The POPA lipids without the water molecules. Right: Only the POPA headgroups are shown. Please visit <http://extras.springer.com/> to view a high-resolution full-color version of this illustration.

2.6. AREA PER MOLECULE AND THICKNESS, COMPARISON TO X-RAY DATA

In homogeneous simulations, the simplest thermodynamic property to calculate is the overall density since we know both the mass and volume of the simulation box for all time steps. The area per molecule and bilayer thickness are two often-calculated membrane quantities, and their values can be extracted from the simulation box volume. In our simulations the area per molecule is determined by dividing the product of the x and y dimensions of a simulation cell by the number of lipids per leaflet. One can also determine the area per molecule by measuring the membrane thickness under the assumption of constant volume per lipid [76].

To determine the membrane thickness, the density profile along the bilayer normal (usually the z -axis), must first be calculated. The density profile can be tabulated by dividing the bilayer into equidistant slabs along the bilayer normal. Each atom is assigned to a slab, and this ensures

that we know again both the mass and the volume of each slab. Density profiles are useful in determining how the locations of different groups (water molecules, lipid headgroups, etc.) vary along the bilayer normal. Because of the short simulation timescales, lipid flip-flop is a rarely witnessed event [77] and hence the density profiles for the top and bottom leaflets of a bilayer can be calculated separately. By looking at the individual leaflet density profiles, one can examine interdigitation, which occurs when lipids from separate leaflets intertwine. This phenomenon has been studied extensively in the context of membrane–alcohol interactions [43,78,79].

The electron density profile can also be determined, and it is a useful simulation measurement because it can be related to X-ray scattering or X-ray reflectivity data since the X-ray profile is essentially a one-dimensional Fourier transform of the electron density [80]. An example of an electron density profile for a POPA lipid bilayer is shown in Figure 2.2. To compare simulation data with that of neutron scattering, an atomic scattering length for all atoms needs to be known so that a scattering length density profile can be assembled.

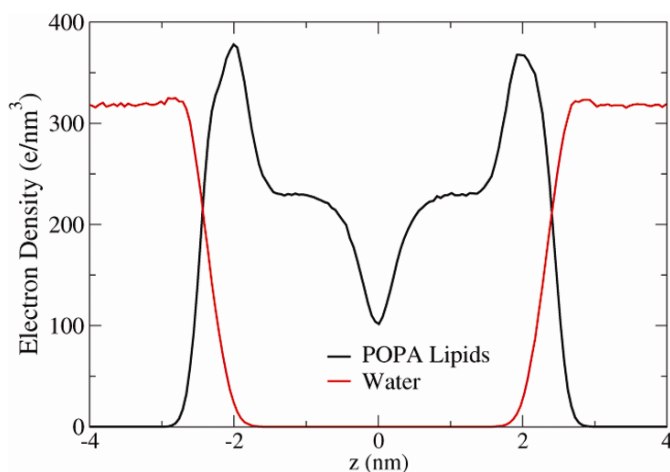


Figure 2.2. Electron density profiles of the POPA lipid bilayer from Figure 2.1. The bilayer center corresponds to a value of $z = 0$ nm. Please visit <http://extras.springer.com/> to view a high-resolution full-color version of this illustration.

2.7. ORDER PARAMETERS AND OTHER SINGLE-LIPID PROPERTIES

Another experimentally relevant parameter is the chain order parameter. This parameter connects the degree of chain ordering to the bilayer normal and, in contrast to the properties previously discussed, the order parameters can be defined for a single lipid. The order parameter is a useful measurement because it can be compared with the experimental deuterium order parameter, which can be determined using nuclear magnetic resonance spectroscopy. Since most atomistic simulations use a united atom representation to model the hydrocarbon chains (even less description is included in coarse-grained systems), hydrogen atoms are not explicitly repre-

sented and the C–H bonds have to be reconstructed assuming a tetrahedral geometry of the CH₂ groups. The order parameter is defined as

$$S_{\text{CD}} = 0.5 \langle 3 \cos^2 \Theta_{\text{CD}} - 1 \rangle, \quad (2.10)$$

where Θ_{CD} is the angle between the CD-bond and the bilayer normal in experiments, and in simulations the CD-bond is replaced by the CH-bond. This quantity cannot be measured directly in experiments; however, there is a recurrent formulation that allows the calculation of S_{CC} from S_{CD} order parameters. For the C_{*n*} groups, the deuterium order parameter for the *n*th carbon in computer simulations can be calculated by

$$-S_{\text{CD}}^n = \frac{2}{3} S_{\text{xx}}^n + \frac{1}{3} S_{\text{yy}}^n.$$

Here $S_{\text{JJ}} = \langle \cos \theta_j \cos \theta_j - \delta_{jj} \rangle$ and ($j = x, y, z$) with $\cos \theta_j = \hat{u}_j \hat{u}_z$, \hat{u}_j is the unit vector for the *j*th molecular axis in the bilayer, and \hat{u}_z is the unit vector in the *z* direction (average bilayer normal). The order parameters are normally defined for all saturated carbons that have two neighboring carbon atoms. For DPPC the order parameters can therefore be calculated for atoms C₂ through C₁₅ (see Fig. 2.3 for numbering). The order parameters for the two hydrocarbon chains are normally analyzed separately, even for DPPC, whose tails each have 16 carbon atoms, because the distance between the two hydrocarbon chains and the water/bilayer interface are not equivalent. For saturated bonds the order parameter is a measure of the spatial restriction of the motion of the C–H vector [81] and is proportional to the deuterium quadrupolar splittings [82] in NMR measurements. For unsaturated bonds (i.e., a double bond) the chain kinks and, although the order parameter can in principle be calculated (nothing in the formula is undefined), it is not usually performed because the local geometry of the atom is not tetrahedral anymore and the values are typically significantly lower than for saturated carbons.

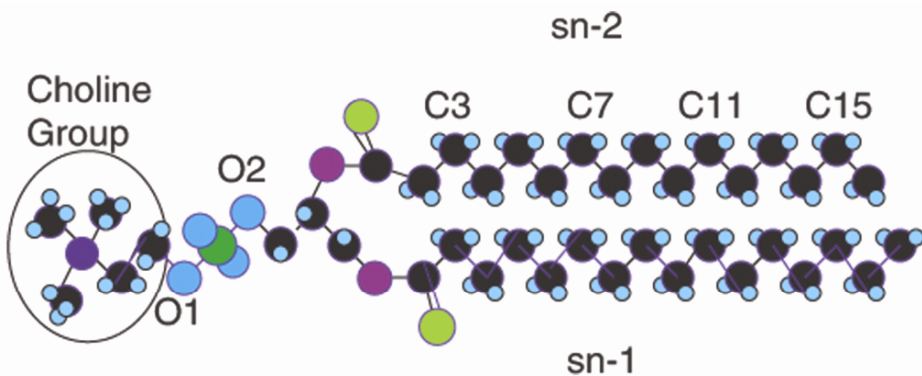


Figure 2.3. An example of how the lipid acyl chains are numbered in calculating the order parameter. The POPA lipid shown here differs from the more commonly studied DPPC lipid in that the DPPC choline group is replaced with a hydrogen atom and the sn-2 tail contains a double bond and 18 atoms. Please visit <http://extras.springer.com/> to view a high-resolution full-color version of this illustration.

There are a number of other properties that describe the intra- and intermolecular conformations of individual lipids. One property is the tilt of the molecule or of the headgroup. To calculate the tilt of the overall molecule, one can define a unit vector that spans from the glycerol group to a specified atom in one of the hydrocarbon chains. To calculate the tilt of the headgroup one can define a unit vector that spans from the choline group to the phosphate group. We can calculate the tilt of the headgroup by measuring the angle of this vector with that of the bilayer normal. The scalar product of the unit vectors (the bilayer normal and the vector of interest) is the cosine of the tilt angle [83]. Another simple way to characterize the structure of a lipid is to calculate its end-to-end distance, i.e., the distance from the headgroup to the end of the tails. This gives a crude estimation of the overall order and phase. For example, the gel phase lipids are normally more ordered than liquid phase lipids and hence have a longer length.

2.8. RADIAL DISTRIBUTION FUNCTIONS

One parameter that can be used to characterize the structure of a molecular modeling system in detail is a radial distribution function (RDF). An RDF provides additional information about the membrane morphology and the structure that is complementary to the density profiles. The RDF ($g_{AB}(r)$) between particles of type A and B is defined as

$$g_{AB} = \frac{\langle \rho_B(r) \rangle}{\langle \rho_B \rangle_{\text{local}}} = \frac{1}{\langle \rho_B \rangle_{\text{local}}} = \frac{1}{N_A \sum_{i,j} N_A N_B} \frac{\delta(r_{i,j} - r)}{4\pi r^2}, \quad (2.11)$$

with $\langle \rho_B(r) \rangle$ being the particle density of type B at a distance r around particle A, and $\langle \rho_B \rangle_{\text{local}}$ the particle density of type B averaged over all spheres around particles A with radius r . Radial distribution functions have two appealing properties. First, they quantitatively describe how many neighbors of a certain type are found around a given atom, and thus they characterize the local neighborhood. Second, the RDFs are a three-dimensional Fourier transform of the static structure factor, which can be measured using either X-rays or neutrons.

For membranes we often only calculate a two-dimensional RDF in order to characterize the in-plane lipid neighborhood. An illustration of an RDF for the POPA example system is shown in [Figure 2.4](#).

2.9. HYDROGEN BONDING AND ADVANCED STATIC ANALYSIS

Since we know the positions and the momenta of all particles at all times in an MD simulation, we have access to all system information. This becomes useful when we want to calculate properties that cannot (or only very indirectly) be determined using experiments. One such example is a study of the hydrogen bonds that exist within a system. A caveat here is that the analysis and the properties are only as good as the model. Hence, for hydrogen bonding studies in atomistic simulations, this means that the hydrogen bond definitions are based on geometry rather than explicit bonding between hydrogen atoms and neighboring polar atoms since that would require the use of quantum degrees of freedom. A typical criterion that we use for hydrogen

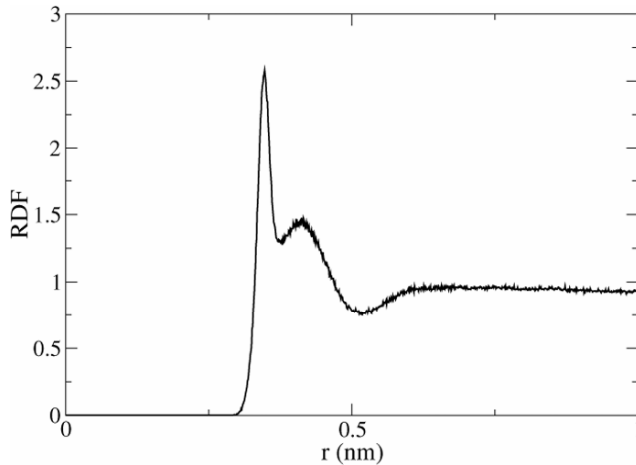


Figure 2.4. The RDF between the water oxygen atoms and the phosphate atom in a POPA lipid bilayer. The figure shows that there are two particularly favorable positions for the water molecules about the phosphate atom. The first location is represented by the sharp peak, which occurs when the water oxygen atom and the phosphate atom are located 0.35 nm apart. The second favorable location occurs at a distance of 0.42 nm and this peak has a smaller g_{AB} value and is much broader than the first peak, indicating that the interaction between the water and the phosphate atom at $r = 0.42$ nm is not as strong as at $r = 0.35$ nm.

bond existence is that the distance between the hydrogen atom and the hydrogen bond acceptor be less than 3.5 \AA and the angle between the hydrogen atom, hydrogen bond donor, and hydrogen bond acceptor be less than 30° [84]. In order to determine the hydrogen bond donor and acceptor pairs, one can assume that an OH or NH group is a good donor and a bare oxygen or nitrogen atom is a good acceptor [77]. Thus, in phospholipid membranes common examples of hydrogen bond acceptors are the oxygen atoms in the phosphate group or the ester groups. To determine the lifetime of a hydrogen bond, one can define a function A that is equal to 1 if a hydrogen bond (in one defined pair) exists and 0 if it does not exist. Based on these values, the hydrogen bond lifetime can be calculated using the function

$$C(t) = \frac{\langle A(t)A(0) \rangle}{\langle A(t)A(t) \rangle}, \quad (2.12)$$

as defined by Luzar and Chandler [85]. Even if a bond does not exist continuously between time 0 and time t , the bond will still be included in the correlation function for the time periods where the bond does exist. In order to calculate the correlation time, we integrate this correlation function:

$$\tau = \int_0^\infty C(t) dt. \quad (2.13)$$

2.10. PRESSURE AND PRESSURE PROFILES

An important thermodynamic property is pressure, which, as discussed earlier, can be kept constant in the three Cartesian directions through the use of a barostat. In an anisotropic medium pressure is not a scalar but a second-rank tensor that is defined in terms of forces, velocities, and positions. When only pair forces exist, the overall pressure is defined as

$$\underline{\underline{P}} = \sum_{\text{pairs}} \vec{F} \otimes \vec{r} + \frac{1}{2} m \vec{v} \otimes \vec{v}. \quad (2.14)$$

If we cannot define all forces based on pair interactions, then we have to be careful about how the origin of the coordinate system is defined when using periodic boundary conditions as the pressure can depend explicitly on this choice. For many applications, the overall pressure calculation, even as a tensor, is not accurate enough, and hence a more localized pressure calculation via formulations such as the Irving-Kirkwood equation are necessary [86]. We do not discuss these methods here but note that one can obtain pressure as a function of position or more often as a function of the position along only the bilayer normal. This is mainly for statistical reasons since pressure can have significantly fluctuating values and good statistics are needed to obtain reliable data. The surface tension can be incorporated into the coupling scheme [77,87] as

$$\int_{Z_1}^{Z_2} \frac{P_r(Z) dZ}{Z_2 - Z_1} = p_{\text{ref}} - \frac{\gamma}{Z_2 - Z_1}, \quad (2.15)$$

with p_{ref} being the chosen reference pressure. An example of a lateral pressure profile is shown in [Figure 2.8](#) for a phosphatidylglycerol system [32].

2.11. TWO-DIMENSIONAL DIFFUSION

Previously, we discussed static and thermodynamic properties of membrane lipids. Since MD gives the user access to particle momenta, we can monitor dynamical properties as well. The lipid mobility is generally examined through the lateral diffusion coefficient, which can be calculated from the slope of the mean-square displacement (MSD) via the Einstein equation:

$$D = \lim_{t \rightarrow \infty} \frac{\langle (r(t) - r(0))^2 \rangle}{2dt}, \quad (2.16)$$

where d is the dimensionality of the system (i.e., $d = 2$ for lateral diffusion in the membrane plane) and $r(t)$ and $r(0)$ are the coordinates of the lipid molecules at times t and 0. An average is calculated for all particles of interest, and over time as a “running-time average” such that an interval of length Δt can be realized from $t = 0$ to $t = \Delta t$, or from $t = t_0$ to $t = t_0 + \Delta t$. Hence, every interval that corresponds to a particular Δt is included in the average. Therefore, after equilibration, all time points are equivalent as reference points. If we have 1000 time steps, this leads to 999 datapoints per particle for a $\Delta t = 1$ versus the existence of only 1 datapoint having a Δt of 999. Thus, the accuracy of the MSD decreases with increasing Δt . As the diffusion coefficient should be calculated from the long time limit of the MSD slope, the accuracy of datapoints from regions corresponding to long Δt values may be questionable. For very short Δt values, the MSD will increase with the square of time according to the equations of motion $\Delta r \propto \Delta t^2$. Sometimes at intermediate Δt values the dynamical regimes may be subdiffusive, resulting in

only long Δt values for calculating diffusive behavior. However, as mentioned above, at long Δt values the MSD may deviate from linearity due to the deteriorated statistical quality. MSDs are regularly plotted double logarithmically in order to easily distinguish the different dynamical regimes; any dynamic regime with algebraic time dependence $\Delta r \propto \Delta t^\alpha$ will then appear as a line with the exponent α equal to the slope. In the case of lipid flip-flop, undulations, or protrusions, one-dimensional MSDs along the bilayer normal are mainly of interest, whereas for water the 3D MSD is usually generated. Figure 2.5 shows how a POPA two-dimensional diffusional coefficient can be derived from the MSD.

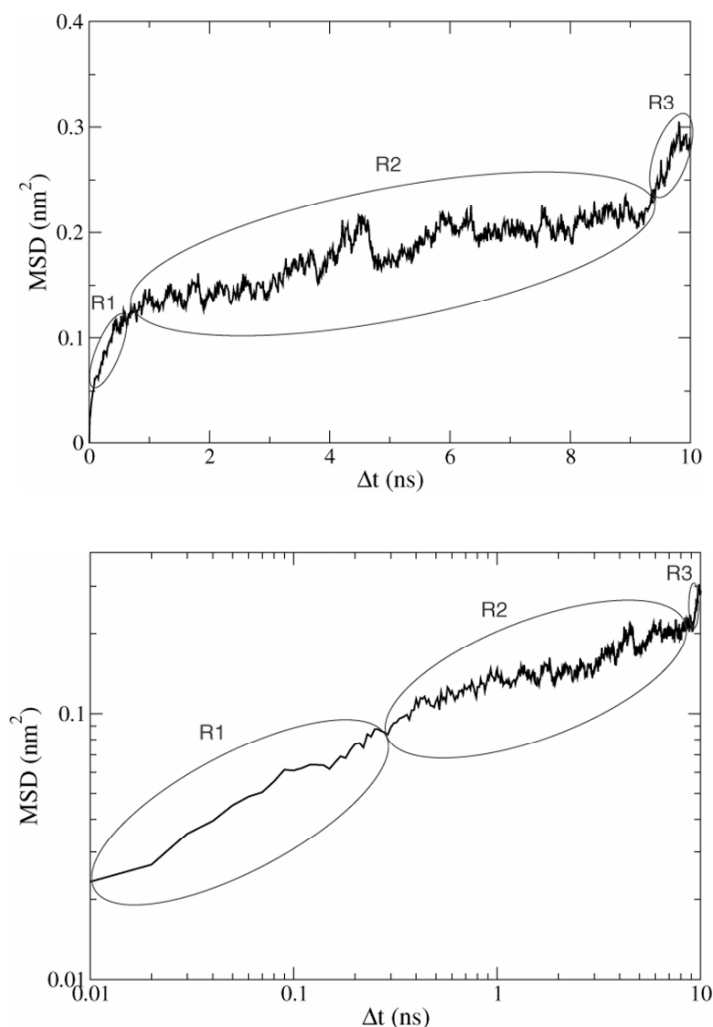


Figure 2.5. A) The lateral mean-squared displacement MSD (in x and y) for POPA. The curve is quadratic for region 1 (R1) since there are no collisions between molecules for small Δt values. The diffusion coefficient can be calculated from the slope of the curve in region 2 (R2) using equation (2.16). The data from region 3 (R3) is not used in calculating the diffusion coefficient because of poor statistics. B) The same data in a log-log plot of the MSD.

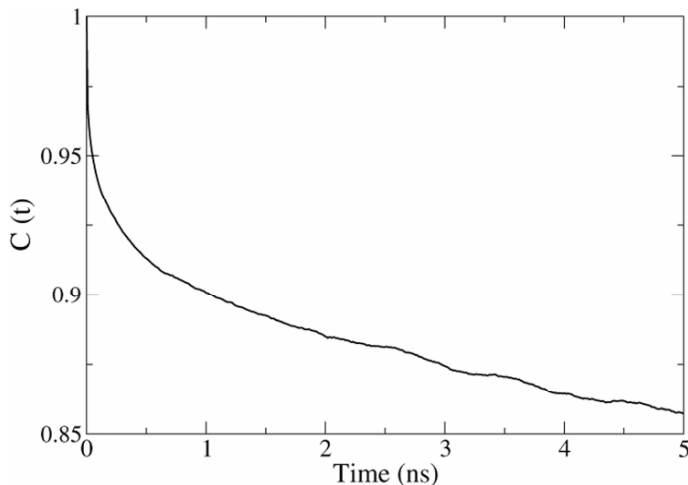


Figure 2.6. An example of a rotational correlation function for the POPA headgroup. Because POPA has such a small headgroup, the vector for this figure spanned only across the phosphate group, from oxygen atom O1 to atom O2 (see Fig. 2.3). For statistical reasons, the correlation function is only calculated for the first 5 ns of a 10 ns trajectory and we can see from the figure that a significantly longer simulation time is required for a complete POPA headgroup relaxation.

2.12. REORIENTATIONS AND NMR

The reorientation of a molecule (e.g., water) and the lipid rotational correlation are also dynamical properties that can be obtained from MD simulations. These parameters require that we either define a plane or a unit vector with which to calculate the reorientation. Since a plane is represented by its normal vector, here we discuss only vector reorientation. The rotational correlation function is calculated using the autocorrelation function for the unit vector \mathbf{V} . Figure 2.6 shows an example of a function, the reorientation of the vector

$$C(t) = \langle \mathbf{V}(t)\mathbf{V}(0) \rangle. \quad (2.17)$$

Other definitions based on higher polynomials can be used as well. The rotational relaxation time τ can again be calculated from the integral of the autocorrelation function (see Eq. (2.13)). This correlation time is related to the T_1 time in NMR experiments [88] as

$$\frac{1}{T_1} = \frac{\hbar^2 \gamma_C^2 \gamma_H^2}{10r_{\text{CH}}^2} [J(\omega_H - \omega_C) + 3J(\omega_C) + 6J(\omega_H + \omega_C)]. \quad (2.18)$$

We restrict ourselves here to CH vectors, but others are equivalent; γ are gyromagnetic ratios of the respective nuclei and ω are the Larmor frequencies, while r is the distance between the nuclei and the J functions are the Fourier transforms of the correlation functions:

$$J(\omega) = \int_{-\infty}^{\infty} C(t) e^{i\omega t} dt. \quad (2.19)$$

We can e.g., use a vector that connects the two tails that measures the in-plane rotation of the lipids since this vector is roughly perpendicular to the long axis of the lipid. Since this vector is nearly perpendicular to the bilayer normal, it decays at long times to a value close to zero. It cannot de-correlate completely since we do not find transbilayer flip-flop on timescales reachable in atomistic simulations. Thus, the correlation function gets stuck at a small nonzero value. The reorientation of the lipid headgroups can be determined by defining a vector that for example spans from the phosphate atom to an atom in the amine or choline groups. This rotation is typically much faster [8] than the rotation of the lipid tails. The rotational correlation vectors of the POPA lipid headgroups are shown in [Figure 2.6](#).

2.13. DYNAMICS OF INDIVIDUAL MOLECULES: CORRELATIONS OF DISTRIBUTION FUNCTIONS

One additional benefit of computer simulations is that the static and dynamical properties of individual molecules can be captured. This selectivity cannot be matched using experiments where typically only average distributions are determined. In studying individual dynamical properties, we essentially do exactly the same calculations that we would perform for an average property, but we restrict ourselves to a small subset. The extreme case of this is a subset with only one member. Another possibility is that we compare spatially or temporally differentiated regions of the bilayer. Far from a phase transition, one typically finds that the average molecule behavior is a reasonable approximation for the individual molecule behavior, i.e., the molecules behave in an essentially identical manner. However, heterogeneities in the system that stem from domain or density differences may be misleading when interpreting individual molecule dynamics, especially when the distribution of lipid behaviors is non-Gaussian and there are qualitative differences between classes. An example is shown in [Figure 2.7](#), where we calculate the rotational correlation function for a simulation of POPA lipids around a protein [89,90]. Each curve displays a set of lipids that is located a different distance from the protein. This is an example of how different observables can be correlated, where the POPA lipid headgroup rotational correlation function value is dependent upon a two-dimensional RDF. Another example could involve classifying lipids into groups of more and less highly ordered lipids based on the individual order parameter values. This lipid separation would then allow additional dynamical properties to be analyzed for each class separately [91]. One word of caution here is that if we investigate the correlation function or the mean-squared displacements of individual lipids, the statistics are very weak and noisy. Thus, an integration of an orientation correlation function to determine a reorientation time or the differentiation of a mean-squared displacement to determine a diffusion coefficient is unreliable.

2.14. INTERACTIONS WITH SMALL MOLECULES

Here, as an example application, we discuss how small molecules modify the behavior of a phospholipid bilayer. Understanding how membranes interact with small molecules is of tremendous biological importance as the cell membrane serves as a barrier between the extracellular environment and the intracellular contents. Therefore, a number of molecular simulations

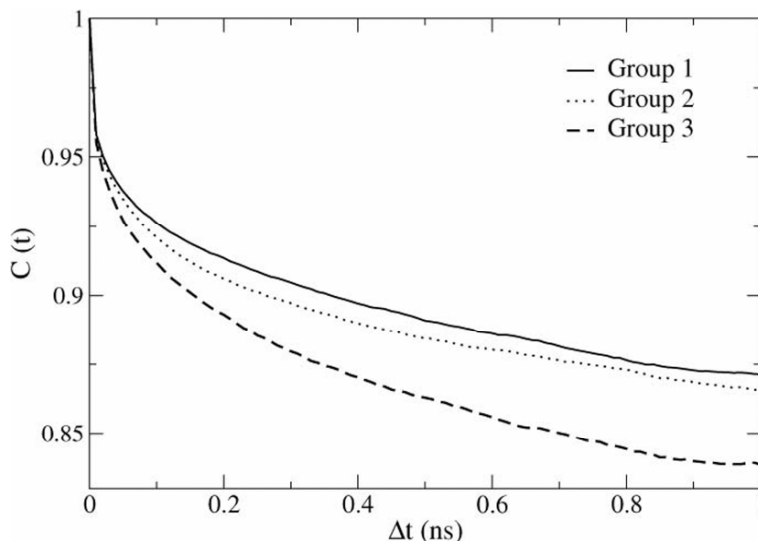


Figure 2.7. This figure shows the rotational correlation function of the POPA lipid head group (vector O7 – O10) for three groups of lipids, where the lipids are sorted into groups based on their lateral root mean squared distance (RMSD) from a transmembrane protein. Group RMSD specifications: Group 1 (<1.0 nm), Group 2 (1.0 nm \leq 2.0 nm), and Group 3 (>2.0 nm) [89].

have been performed on systems that contain lipid bilayers and small molecules [7,9,43,77,78,92,93]. Among the small molecules that have been studied are sugars and alcohols. Sugar molecules are nutrients for living organisms; under the proper conditions they can serve as cryoprotectants [94–96]. In particular, trehalose, which is a disaccharide of glucose, has been found to be very effective in this respect. Recently, it has been shown that the molecular mechanism underlying this cryoprotective effect is a result of hydrogen bonding between the trehalose molecules and the bilayer headgroups [7]. The sugar can replace some of the hydrogen bonds that normally form between the water molecules and the bilayer headgroups and thereby stabilize the fragile bilayer structure. Stabilization here means that the bilayer is able to withstand harsher environmental conditions in the presence of small molecules when compared with a single-lipid bilayer in water. Experimentally, it has been shown that trehalose prevents lipids from undergoing a phase transition under cooling, i.e., it shifts the main-phase transition temperature significantly [97]. Simulations have in general been able to corroborate these effects [92,98].

It has been found experimentally that alcohol molecules have the opposite effect of trehalose and destabilize model membranes [99,100]. It has been observed that upon the addition of alcohol molecules the lipid bilayer becomes thinner and the area per molecule increases. One application for alcohol/membrane experiments is that of stuck fermentations in the wine industry [101,102]. In a stuck fermentation, the yeast cells do not convert all available sugar molecules into alcohol but stop at an incomplete stage. It has been proposed that the underlying mechanism of stuck fermentations is an alcohol-triggered structural transition in the membrane that results in conformational changes to transmembrane proteins that render them dysfunctional [101,103]. Aside from wine production, increased sugar conversion would also be beneficial in the production of ethanol as a component in biofuels. Furthermore, alcohols have been

used as model anesthetic molecules where it has been proposed that anesthetic molecules may alter the lateral pressure profile of lipids, again resulting in conformational changes to transmembrane proteins [104,105]. An example of a lateral pressure profile is shown in Figure 2.8 for a phosphatidylglycerol system.

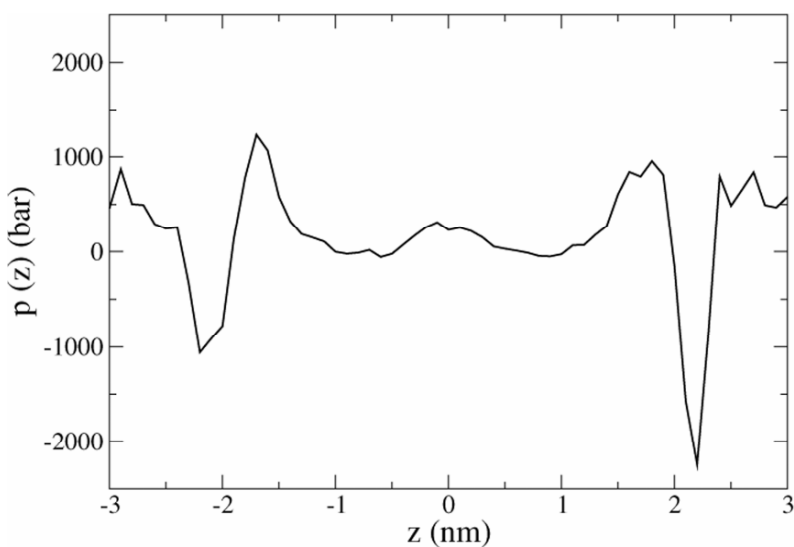


Figure 2.8. Lateral Pressure Profile for a 128 lipid POPG bilayer³². The asymmetry of the figure is due to statistical sampling deficiencies. We can clearly identify the headgroup water interfaces by the large peaks.

2.15. SUMMARY

It is clear that biomolecular modeling in general and molecular dynamics of biomembranes in particular is an efficient and useful tool to understand lipid bilayer systems. No other technique allows us to access all atom positions directly and offers in that way an unprecedented and unrivalled degree of detail. The question of modeling biomolecules is therefore no longer a “Why” or “If” but a “How.” In this chapter we could only give a brief overview of the fundamentals of the technique. We could not discuss the statistical mechanical fundamentals of molecular dynamics. There are, however, many excellent books on that. We rather wanted to deliver a brief introduction that can be rapidly implemented by the non-expert user as molecular modeling starts to become a tool that is not only used by experts who devote their full time and often whole career to it. But due to the abundance and reliability of modern software packages, it can often be used as a tool for a short side project without going into all the depths.

Nonetheless, as with any other technique there are several traps that need to be avoided. It is a danger of modern software packages that they provide default values for almost all switches and numbers to be chosen in a simulation such that the user is tempted not to think about settings at all. We wanted therefore to explain the meaning of the most important of these often

elusive settings that can fail simulations. The failure of a simulation is often not very obvious; if it crashes and the software aborts we know we did something wrong. But often simulations do not crash but are completely meaningless because the software is used in an inadequate manner; and for computers we must keep one thing in mind: they do *exactly* what they are programmed to do, not what we think we programmed them to do. So the two main ideas we wanted to convey here are that nobody should be dissuaded from using molecular modeling because of a fear of its complexity and that there are a few points about which one really has to be careful.

In general, simulations in many cases offer a very good visual understanding of a system where other techniques may be more precise. The strength of a simulation is most often in its interplay with other, mainly experimental, techniques. Simulations complement experiments by providing access to the mechanisms on a molecular level that give rise to experimental observables. The numbers themselves may often be only qualitative, but a mechanistic understanding is an invaluable asset.

ACKNOWLEDGMENTS

We would like to thank our former and current collaborators for many stimulating discussions. Funding was partially provided by NIH (NIH-NIGMS Grant Number T32-GM08799) and NSF (Grant Number CBET 0506602).

PROBLEMS

Simulations are a useful method for studying how molecule location and orientation are influenced by the positions of neighboring molecules and the local environment. If you happen to have access to a Unix/Linux computer and can download the MD simulation program Gromacs (<http://www.gromacs.org/>), complete Exercise 2.1 to simulate a solvated lipid bilayer and analyze the resulting water molecule orientations. If you do not have such access, use the resulting simulation data from Exercise 2.1 (available for download at <http://www.chms.ucdavis.edu/research/web/faller/downloads.html>) and proceed with the data analysis portion of the problem.

Preparing the Simulation Program

Download Gromacs. In this exercise, the syntax for the input will correspond to Gromacs version 3.3.1.

We are interested in comparing the molecular ordering between water molecules that are located close to a lipid bilayer surface and bulk-like water molecules.

Follow the steps below to generate a hydrated lipid bilayer

- a. Make a new directory and name it lipid
- b. Go to http://moose.bio.ucalgary.ca/index.php?page=Structures_and_Topologies and download the *dppc128.pdb* file. Save this file in your lipid directory
- c. Download the *dppc.itp* and *lipid.itp* files into your directory
- d. Download the *example2.top* file and rename it *topol.top*
- e. Copy the *grompp.mdp* file from */share/tutor/water* into your directory

- f. Use the command `editconf -f dppc128.pdb -o conf.gro` to convert your configuration file into a .gro file format
- g. Change the number of time steps in the `grompp.mdp` file from 10,000 to 250,000
- h. Run the `grompp` and `mdrun` commands. This will generate a trajectory that is 0.5 ns in length since the time step in the `grompp.mdp` file is 2 fs.
- i. When the simulation is complete you will see a `confout.gro` file,
- j. An index file needs to be created to specify which atom in the water molecule is of interest. We will choose the oxygen atom, which is labeled OW.
- k. Type the command `make_ndx -f conf.gro -o index.ndx`. A prompt will open and ask you to specify the atom of interest. Type `2 & a OW` to specify the oxygen atom in water. Then enter `q` to exit.
- l. Calculate the radial distribution function with `g_rdf -n index.ndx`. You will be asked to specify two groups. Since we are interested in the water oxygen atoms, choose “3” twice. The results are in `rdf.xvg`.

Water Box

- a. Make a new folder and name it `waterbox`
- b. Copy the `topol.top` and `grompp.mdp` files from the lipid directory into the `waterbox` directory.
- c. We need to make a new configuration file that contains only water molecules. Type `genbox -cs -box 6.41840 6.44350 2.67 -o conf.gro`. This creates a box of 3652 water molecules, where the x and the y box lengths are the same as those in the lipid simulation `conf.gro` file.
- d. In the `topol.top` file, delete the line that says “DPPC 128” and change the number of water molecules to 3652.
- e. Run the `grompp` and `mdrun` commands.
- f. Make a new index file with `make_ndx -f conf.gro -o index.ndx`. A prompt will open and ask you to specify the atom of interest. Type `1 & a OW` to specify the oxygen atom in water. Then enter `q` to exit.
- g. Calculate the radial distribution function with `g_rdf -n index.ndx`. You will be asked to specify two groups. Since we are interested in the water oxygen atoms, choose “2” twice.

Exercise 2.1

Plot the resulting radial distribution functions (RDFs) on the same graph. Discuss the differences between the resulting RDFs from the two systems. Are the water molecules more or less ordered near the surface? How would the RDF differ if we simulated water molecules near a smooth surface rather than a bilayer? Based on the definition of an RDF, why do the RDF values approach 1 with an increase in molecular distance?

You can now repeat the steps for the POPA layer discussed in this chapter in detail. The necessary configuration/topology files can be found at:

<http://www.chms.ucdavis.edu/research/web/faller/downloads.html>.

FURTHER STUDY

Molecular Dynamics and Other Modeling Techniques in General

Allen MP, Tildesley DJ. 1987. *Computer simulation of liquids*. Oxford: Clarendon Press.

Frenkel D, Smit B. 1996. *Understanding molecular simulation: from basic algorithms to applications*. San Diego: Academic Press.

Leach A. 1997. *Molecular modelling: principles and applications*. Essex: Addison Wesley.

Specific Software Packages and Force Fields

Gromos/Gromacs

van Gunsteren WF, Billeter SR, Eising AA, Hünenberger P, Krüger AE, Mark WRP, Scott AE, Tironi IG. 1996. *Biomolecular simulation: the GROMOS manual and user guide*. Zürich: Vdf.

Lindahl E, Hess B, van der Spoel D. 2001. GROMACS 3.0: a package for molecular simulation and trajectory analysis. *J Mol Model* **7**(8):306–317.

Hess B, Kutzner C, van der Spoel D, Lindahl E. 2008. GROMACS 4: algorithms for highly efficient, load-balanced, and scalable molecular simulation. *J Chem Theor Comput* **4**(3):435–447.

<http://www.gromacs.org>

Charmm

Brooks BR, Bruccoleri RE, Olafson DJ, States DJ, Swaminathan S, Karplus M. 1983. CHARMM: a program for macromolecular energy, minimization, and dynamics calculations. *J Comput Chem* **4**:187–217.

MacKerel Jr AD, Brooks III CL, Nilsson L, Roux B, Won Y, Karplus M. 1998. CHARMM: the energy function and its parameterization with an overview of the program. In *The Encyclopedia of Computational Chemistry*, Vol. 1, pp. 271–277. Ed. PvR Schleyer. Chichester: John Wiley & Sons.

<http://www.charmm.org>

Amber

Cornell WD, Cieplak P, Bayly CI, Gould IR, Merz KM, Ferguson DM, Spellmeyer DC, Fox T, Caldwell JW, Kollman PA. 1995. A second generation force field for the simulation of proteins, nucleic acids, and organic molecules. *J Am Chem Soc* **117**(19):5179–5197.

<http://amber.scripps.edu/>

REFERENCES

1. Verlet L. 1967. Computer ‘experiments’ on classical fluids, I: thermodynamical properties of Lennard-Jones molecules. *Phys Rev* **159**:98–103.
2. Allen MP, Tildesley DJ. 1987. *Computer simulation of liquids*. Oxford: Clarendon Press.
3. Frenkel D, Smit B. 1996. *Understanding molecular simulation: from basic algorithms to applications*. San Diego: Academic Press.
4. Leach A. 1997. *Molecular modelling: principles and applications*. Essex: Addison Wesley.
5. Egberts E, Marrink S-J, Berendsen HJC. 1994. Molecular dynamics simulation of a phospholipid membrane. *Eur Biophys J* **22**:423–436.
6. Tieleman DP, Marrink SJ, Berendsen HJC. 1997. A computer perspective of membranes: molecular dynamics studies of lipid bilayer systems. *Biochim Biophys Acta* **1331**:235–270.
7. Sum AK, Faller R, de Pablo JJ. 2003. Molecular simulation study of phospholipid bilayers and insights of the interactions with disaccharides. *Biophys J* **85**:2830–2844.

8. Faller R, Marrink S-J. 2004. Simulation of domain formation in mixed DLPC–DSPC lipid bilayers. *Langmuir* **20**:7686–7693.
9. Lee BW, Faller R, Sum AK, Vattulainen I, Patra M, Karttunen M. 2004. Structural effects of small molecules on phospholipid bilayers investigated by molecular simulations. *Fluid Phase Equilib* **225**:63–68.
10. Switzer J, Bennun S, Longo ML, Palazoglu A, Faller R. 2006. Karhunen-Loeve analysis for pattern description in phase separated lipid bilayer systems. *J Chem Phys* **124**:234906.
11. Cooke IR, Kremer K, Deserno M. 2005. Tunable generic model for fluid bilayer membranes. *Phys Rev E* **72**:011506.
12. Moore PB, Lopez CF, Klein ML. 2001. Dynamical properties of a hydrated lipid bilayer from a multianosecond molecular dynamics simulation. *Biophys J* **81**:2484–2494.
13. Lopez CF, Nielsen SO, Moore PB, Shelley JC, Klein ML. 2002. Self-assembly of a phospholipid Langmuir monolayer using coarse-grained molecular dynamics simulations. *J Phys Condens Matter* **14**:9431–9444.
14. Patra M, Karttunen M, Hyvönen MT, Falck E, Vattulainen I. 2004. Lipid bilayers driven to a wrong plane in molecular dynamics simulations by truncation of long-range electrostatic interactions. *J Phys Chem B* **108**:4485–4494.
15. Feller SE, Pastor RW, Rojnuckarin A, Bogusz S, Brooks BR. 1996. Effect of electrostatic force truncation on interfacial and transport properties of water. *J Phys Chem* **100**:17011–17020.
16. Anezo C, de Vries AH, Holtje H, Tieleman DP, Marrink SJ. 2003. Methodological issues in lipid bilayer simulations. *J Phys Chem B* **107**:9424–9433.
17. Farago O. 2003. "Water-free" computer model for fluid bilayer membranes. *J Chem Phys* **119**:596–605.
18. Marrink SJ, de Vries AH, Mark AE. 2004. Coarse grained model for semi-quantitative lipid simulation. *J Phys Chem B* **108**:750–760.
19. Stevens MJ. 2004. Coarse-grained simulations of lipid bilayers. *J Chem Phys* **121**:11942–1198.
20. Shelley JC, Shelley MY, Reeder RC, Bandyopadhyay S, Klein ML. 2001. A coarse grain model for phospholipid simulations. *J Phys Chem B* **105**:4464–4470.
21. Kaznessis YN, Kim ST, Larson RG. 2002. Simulations of zwitterionic and anionic phospholipid monolayers. *Biophys J* **82**:1731–1742.
22. Alper HE, Bassolino D, Stouch TR. 1993. Computer simulation of a phospholipid monolayer-water system: the influence of long-range forces on water structure and dynamics. *J Chem Phys* **98**:9798–9807.
23. Feller SE, Zhang YH, Pastor RW. 1995. Computer-simulation of liquid/liquid interfaces, II: surface-tension area dependence of a bilayer and a monolayer. *J Chem Phys* **103**:10267–10276.
24. Heine DR, Rammohan AR, Balakrishnan J. 2007. Atomistic simulations of the interaction between lipid bilayers and substrates. *Mol Simul* **33**:391–397.
25. Xing C, Faller R. 2008. Interactions of lipid bilayers with supports: a coarse-grained molecular simulation study. *J Phys Chem B* **112**:7086–7094.
26. Berendsen HJC, Postma JPM, van Gunsteren WF, Dinola A, Haak JR. 1984. Molecular dynamics with coupling to an external bath. *J Chem Phys* **81**:3684–3690.
27. Essman U, Perela L, Berkowitz ML, Darden HLT, Pedersen LG. 1995. A smooth particle mesh Ewald method. *J Chem Phys* **103**:8577–8592.
28. Mashl RJ, Scott HL, Subramaniam S, Jakobsson E. 2001. Molecular simulation of dioleoylphosphatidylcholine lipid bilayers at differing levels of hydration. *Biophys J* **81**:3005–3015.
29. Feller SE, Yin D, Pastor RW, MacKerel Jr. AD. 1997. Molecular dynamics simulation of unsaturated lipid bilayers at low hydration: parameterization and comparison with diffraction studies. *Biophys J* **73**:2269–2279.
30. Tieleman DP, Berendsen HJC. 1996. Molecular dynamics simulations of fully hydrated dipalmitoylphosphatidylcholine bilayer with different macroscopic boundary conditions and parameters. *J Chem Phys* **105**:4871–4880.
31. Balali-Mood K, Harroun TA, Bradshaw JP. 2003. Molecular dynamics simulations of a mixed DOPC/DOPG bilayer. *Eur Phys J E* **12**:S135–S140.
32. Dickey A, Faller R. 2008. Examining the contributions of lipid shape and headgroup charge on bilayer behavior. *Biophys J* **95**:2636–2646.
33. Berger O, Edholm O, Jahnig F. 1997. Molecular dynamics simulations of a fluid bilayer of dipalmitoylphosphatidylcholine at full hydration, constant pressure, and constant temperature. *Biophys J* **72**:2002–2013.
34. Pandit SA, Bostick D, Berkowitz ML. 2003. Mixed bilayer containing dipalmitoylphosphatidylcholine and dipalmitoylphosphatidylserine: lipid complexation, ion binding, and electrostatics. *Biophys J* **85**:3120–3131.

35. Niemela P, Hyvonen MT, Vattulainen I. 2004. Structure and dynamics of sphingomyelin bilayer: insight gained through systematic comparison to phosphatidylcholine. *Biophys J* **87**:2976–2989.
36. Pandit SA, Jakobsson E, Scott HL. 2004. Simulation of the early stages of nano-domain formation in mixed bilayers of sphingomyelin, cholesterol, and dioleoylphosphatidylcholine. *Biophys J* **87**:3312–3322.
37. Murzyn K, Rog T, Pasienkiewicz-Gierula M. 2005. Phosphatidylethanolamine–phosphatidylglycerol bilayer as a model of the inner bacterial membrane. *Biophys J* **88**:1091–1103.
38. Leekumjorn S, Sum AK. 2006. Molecular simulation study of structural and dynamic properties of mixed DPPC/DPPE Bilayers. *Biophys J* **90**:3951–3965.
39. Gurtovenko A, Patra M, Karttunen M, Vattulainen I. 2004. Cationic DMPC/DMTAP lipid bilayers: molecular dynamics study. *Biophys J* **86**:3461–3472.
40. Falck E, Patra M, Karttunen M, Hyvonen MT, Vattulainen I. 2004. Lessons of slicing membranes: interplay of packing, free area and lateral diffusion in phospholipid/cholesterol bilayers. *Biophys J* **87**:1076–1091.
41. Pandit SA, Bostick D, Berkowitz ML. 2004. Complexation of phosphatidylcholine lipids with cholesterol. *Biophys J* **86**:1345–1356.
42. Smondryev AM, Berkowitz ML. 2001. Molecular dynamics simulation of the structure of dimyristoylphosphatidylcholine bilayers with cholesterol, ergosterol and lanosterol. *Biophys J* **80**:1649–1658.
43. Dickey AN, Yim W-S, Faller R. 2009. Using ergosterol to mitigate the deleterious effects of ethanol on bilayer structure. *J Phys Chem B*. **113**:2388–2397.
44. Hess B, Bekker H, Berendsen HJC, Fraaije JGEM. 1997. LINCS: a linear constraint solver for molecular simulations. *J Comput Chem* **18**:1463–1472.
45. Müller-Plathe F, Brown D. 1991. Multi-colour algorithms in molecular simulation: vectorisation and parallelisation of internal forces and constraints. *Comput Phys Commun* **64**:7–14.
46. Berendsen HJC, Postma JPM, van Gunsteren WF, Hermans J. 1981. Interaction models for water in relation to protein hydration. In *Intermolecular forces*, pp. 331–342. Ed. B Pullman. Dordrecht: Reidel.
47. Berendsen HJC, Grigera JR, Straatsma TP. 1987. The missing term in effective pair potentials. *J Phys Chem* **91**:6269–6271.
48. Mackerel AD. 2004. Empirical force fields for biological macromolecules: overview and issues. *J Comput Chem* **25**:1584–1604.
49. Aman K, Lindahl E, Edholm O, Hakansson P, Westlund PO. 2003. Structure and dynamics of interfacial water in an L-alpha phase lipid bilayer from molecular dynamics simulations. *Biophys J* **84**:102–115.
50. Pasenkiewicz-Gierula M, Takaoka Y, Miyagawa H, Kitamura K, Kusumi A. 1999. Charge pairing of headgroups in phosphatidylcholine membranes: a molecular dynamics simulation study. *Biophys J* **76**:1228–1240.
51. Tieleman DP, Berendsen HJC. 1996. Molecular dynamics simulations of a fully hydrated dipalmitoyl phosphatidylcholine bilayer with different macroscopic boundary conditions and parameters. *J Chem Phys* **105**:4871–4880.
52. Hofsass C, Lindahl E, Edholm O. 2003. Molecular dynamics simulations of phospholipid bilayers with cholesterol. *Biophys J* **84**:2192–2206.
53. Tu KC, Klein ML, Tobias DJ. 1998. Constant-pressure molecular dynamics investigation of cholesterol effects in a dipalmitoylphosphatidylcholine bilayer. *Biophys J* **75**:2147–2156.
54. Muller M, Katsov K, Schick M. 2006. Biological and synthetic membranes: what can be learned from a coarse-grained description? *Phys Rep* **434**:113–176.
55. Shelley JC, Shelley MY, Reeder RC, Bandyopadhyay S, Moore PB, Klein ML. 2001. Simulations of phospholipids using a coarse grain model. *J Phys Chem B* **105**:9785–9792.
56. Shelley JC, Shelley MY, Reeder RC, Bandyopadhyay S, Klein ML. 2001. A coarse grain model for phospholipid simulations. *J Phys Chem B* **105**:4464–4470.
57. Nielsen SO, Lopez CF, Srinivas G, Klein ML. 2004. Coarse grain models and the computer simulation of soft materials. *J Phys Condens Matter* **16**:R481–R512.
58. Marrink SJ, Risselada J, Mark AE. 2005. Simulation of gel phase formation and melting in lipid bilayers using a coarse grained model. *Chem Phys Lipids* **135**:223–244.
59. Marrink SJ, Mark AE. 2004. Molecular view of hexagonal phase formation in phospholipid membranes. *Biophys J* **87**:3894–3900.
60. Lopez CF, Moore PB, Shelley JC, Shelley MY, Klein ML. 2002. Computer simulation studies of biomembranes using a coarse grain model. *Comput Phys Commun* **147**:1–6.

61. Marrink SJ, Risselada HJ, Yefimov S, Tieleman DP, de Vries AH. 2007. The MARTINI force field: coarse grained model for biomolecular simulations. *J Phys Chem B* **111**:7812–7824.
62. Bennun SV, Longo ML, Faller R. 2007. Phase and mixing behavior in two-component lipid bilayers: a molecular dynamics study in DLPC/DSPC mixtures. *J Phys Chem B* **111**:9504–9512.
63. Marrink SJ, Mark AE. 2003. Molecular dynamics simulation of the formation, structure, and dynamics of small phospholipid vesicles. *J Am Chem Soc* **125**:15233–15242.
64. Faller R, Marrink SJ. 2004. Simulation of domain formation in DLPC–DSPC mixed bilayers. *Langmuir* **20**:7686–7693.
65. Bennun SV, Longo M, Faller R. Molecular scale structure in fluid-gel patterned bilayers: stability of interfaces and transmembrane distribution. To be submitted.
66. Bennun S, Longo ML, Faller R. 2007. The molecular scale structure in fluid-gel patterned bilayers: stability of interfaces and transmembrane distribution. *Langmuir* **23**:12465–12468.
67. Brannigan G, Brown FLH. 2004. Solvent-free simulations of fluid membrane bilayers. *J Chem Phys* **120**:1059–1071.
68. Noguchi H, Takasu M. 2001. Self-assembly of amphiphiles into vesicles: a Brownian dynamics simulation. *Phys Rev E* **64**:041913.
69. Reynwar BJ, Illya G, Harmandaris VA, Müller MM, Kremer K, Deserno M. 2007. Aggregation and vesiculation of membrane proteins by curvature-mediated interactions. *Nature* **447**:461–467.
70. Harmandaris VA, Deserno M. 2006. A novel method for measuring the bending rigidity of model lipid membranes by simulating tethers. *J Chem Phys* **125**:204905.
71. Weeks JD, Chandler D, Andersen HC. 1971. Role of repulsive forces in determining the equilibrium structure of simple liquids. *J Chem Phys* **54**:5237–5247.
72. Faller R, Kuhl TL. 2003. Modeling the binding of cholera-toxin to a lipid membrane by a non-additive two-dimensional hard disk model. *Soft Mater* **1**:343–352.
73. Majewski J, Kuhl TL, Kjaer K, Smith GS. 2001. Packing of ganglioside-phospholipid monolayers: an x-ray diffraction and reflectivity study. *Biophys J* **81**:2707–2715.
74. Humphrey W, Dalke A, Schulten K. 1996. VMD—visual molecular dynamics. *J Mol Graphics* **14**:33–38.
75. Sayle RA, Milner-White EJ. 1995. RASMOL: biomolecular graphics for all. *Trends Biochem Sci* **20**:374–376.
76. Pandit SA, Chiu S-W, Jakobsson E, Grama A, Scott HL. 2007. Cholesterol surrogates: a comparison of cholesterol and 16:0 ceramide in POPC bilayers. *Biophys J* **92**:920–927.
77. Dickey AN, Faller R. 2007. How alcohol chain-length and concentration modulate hydrogen bond formation in a lipid bilayer. *Biophys J* **92**:2366–2376.
78. Dickey AN, Faller R. 2005. Investigating interactions of biomembranes and alcohols: a multiscale approach. *J Polym Sci B* **43**:1025–1032.
79. Kranenburg M, Venturoli M, Smit B. 2003. Phase behavior and induced interdigitation in bilayers studied with dissipative particle dynamics. *J Phys Chem B* **107**:11491–11501.
80. Miller CE, Majewski J, Gog T, Kuhl TL. 2005. Characterization of biological thin films at the solid–liquid interface by x-ray reflectivity. *Phys Rev Lett* **94**:238104.
81. Tieleman DP, Marrink SJ, Berendsen HJC. 1997. A computer perspective of membranes: molecular dynamics studies of lipid bilayer systems. *Biochim Biophys Acta* **1331**:235–270.
82. Davis JH. 1983. The description of membrane lipid conformation, order and dynamics by ²H-NMR. *Biochim Biophys Acta* **737**:117–171.
83. Aittoniemi J, Róg T, Niemela P, Pasenkiewicz-Gierula M, Vattulainen I, Karttunen M. 2006. Sterol tilt: major determinant of sterol ordering capability in lipid membranes. *J Phys Chem B Lett* **110**:25562–25564.
84. Lindahl E, Hess B, van der Spoel D. 2001. GROMACS 3.0: a package for molecular simulation and trajectory analysis. *J Mol Model* **7**:306–317.
85. Luzar A, Chandler D. 1996. Hydrogen-bond kinetics in liquid water. *Nature* **379**:55–57.
86. Ollila S, Hyvonen MT, Vattulainen I. 2007. Polyunsaturation in lipid membranes: dynamic properties and lateral pressure profiles. *J Phys Chem B* **111**:3139–3150.
87. Chiu SW, Clark M, Balaji V, Subramaniam S, Scott HL, Jakobsson E. 1995. Incorporation of surface tension into molecular dynamics simulation of an interface: a fluid phase lipid bilayer membrane. *Biophys J* **69**:1230–1245.
88. Schmidt-Rohr K, Spiess HW. 1994. *Multidimensional solid state NMR and polymers*. New York: Academic Press.

89. Dickey AN, Faller R. 2008. Behavioral differences between phosphatidic acid and phosphatidylcholine in the presence of the nicotinic acetylcholine receptor. *Biophys J* **95**:2636–2646.
90. Dickey AN. 2008. How bilayer composition affects the stability of a model yeast membrane and the behavior of lipids surrounding the nicotinic acetylcholine receptor. PhD dissertation. University of California Davis.
91. Wong BY, Faller R. 2007. Phase behavior and dynamic heterogeneities in lipids: a coarse-grained simulation study of DPPC–DPPE mixtures. *Biochim Biophys Acta* **1768**:620–627.
92. Sum AK, Faller R, de Pablo JJ. 2003. Molecular simulation study of phospholipid bilayers and insights of the interactions with disaccharides. *Biophys J* **85**:2830–2844.
93. Patra M, Salonen E, Terama E, Vattulainen I, Faller R, Lee BW, Holopainen J, Karttunen M. 2006. Under the influence of alcohol: the effect of ethanol and methanol on lipid bilayers. *Biophys J* **90**:1121–1135.
94. Crowe JH, Crowe LM, Carpenter JF, Rudolph AS, Wistrom CA, Spargo BJ, Anchordoguy TJ. 1988. Interactions of sugars with membranes. *Biochim Biophys Acta* **947**:367–384.
95. Crowe JH, Crowe LM, Carpenter JF, Wistrom CA. 1987. Stabilization of dry phospholipid bilayers and proteins by sugar. *Biochem J* **242**:1–10.
96. Crowe JH, Crowe LM, Oliver AE, Tsvetkova N, Wolkers W, Tablin F. 2001. The trehalose myth revisited: introduction to a symposium on stabilization of cells in the dry state. *Cryobiology* **43**:89–105.
97. Crowe JH, Crowe LM, Chapman D. 1984. Preservation of membranes in anhydrobiotic organisms: the role of trehalose. *Science* **223**:701–703.
98. Pereira CS, Lins RD, Chandrasekhar I, Carlos L, Freitas G, Hünenberger PH. 2004. Interaction of the disaccharide trehalose with a phospholipid bilayer: a molecular dynamics study. *Biophys J* **86**:2273–2285.
99. Ly HV, Block DE, Longo ML. 2002. Interfacial tension effect of ethanol on lipid bilayer rigidity, stability, and area/molecule: a micropipet aspiration approach. *Langmuir* **18**:8988–8995.
100. Ly HV, Longo ML. 2004. The influence of short-chain alcohols on interfacial tension, mechanical properties, area/molecule, and permeability of fluid lipid bilayers. *Biophys J* **87**:1013–1033.
101. Bisson LF, Block DE. 2002. Ethanol tolerance in *Saccharomyces*. In *Biodiversity and biotechnology of wine yeasts*, pp. 85–98. Ed. M Ciani. Trivandrum, India: Research Signpost.
102. Cramer AC, Vlassides S, Block DE. 2002. Kinetic model for nitrogen-limited wine fermentations. *Biotechnol Bioeng* **77**:49–60.
103. Bisson LF. 1999. Stuck and sluggish fermentations. *Am J Enol Vitic* **50**:107–119.
104. Cantor RS. 1997. The lateral pressure profile in membranes: a physical mechanism of general anesthesia. *Biochemistry* **36**:2339–2344.
105. Terama E, Ollila OH, Salonen E, Rowat AC, Trandum C, Westh P, Patra M, Karttunen M, Vattulainen I. 2008. Influence of ethanol on lipid membranes: from lateral pressure profiles to dynamics and partitioning. *J Phys Chem B* **112**:4131–4139.